PCCP

Accepted Manuscript

ROYAL SOCIETY OF CHEMISTRY

www.rsc.org/pccp

Comparing induced point-dipoles and Drude oscillators

Michael Schmollngruber,[1] Volker Lesch,[2] Christian Schröder,[1, a)] Andreas Heuer,[2] and Othmar Steinhauser[1]
[1)] *University of Vienna, Department of Computational Biological Chemistry, Austria*
[2)] *Westfälische Wilhelms-Universität Münster, Insitute of Physical Chemistry, Germany*

(Dated: 5 November 2014)

Classical Molecular Dynamics simulations describing electrostatic interactions only by point charges can be augmented by the inclusion of atomic polarisabilities modelling charge flexibility. Two widely used models, Drude oscillators and induced point-dipoles, are compared in a systematic study using their respective implementations in CHARMM and AMBER. The question of necessity and importance of polarisable hydrogen atoms is raised and two implementations, in an implicit or explicit manner, are compared to the case of non-polarisable hydrogen atoms. For all these polarisability models, the strength of the respective atomic polarisabilities was incremented in steps of ten percent up to their full values. The influence of polarisability on the structure and dynamics of the ionic liquid $EMIM^{\oplus}CF_3SO_3^{\ominus}$, which is chosen as a test case, is studied thoroughly. Using appropriate model functions, the respective dynamical and structural data are fitted. Thus, a small set of parameters is deduced, which highlights the effect of polarisability. Generally, flexibility of the charge distribution leads to enhanced fluidity and less pronounced structure. As this usually occurs when adding a co-solvent to an ionic liquid, the inclusion of polarisability can be seen in much the same way in that it acts like an inner solvent.

Keywords: ionic liquid, polarisability, molecular dynamics, Drude, point-dipole, simulation

I. INTRODUCTION

Computer simulations of soft matter have a long tradition.[1] In order to cope with the complexity of the problem, i.e. system size, simulation length and sufficient sampling, interaction potentials have to be designed which are both, realistic as well as economic.[2] For this reason, the electrostatic part of interaction is traditionally described by a set of permanent point charges.[3] This prohibits, however, the reaction of a molecular charge distribution to changes of its environment. Recent years have seen a development of models to introduce flexible charge distributions, thus augmenting traditional molecular mechanics force fields. Three principal methods have evolved in the literature.[4]

On the one hand, the strength of the charges may fluctuate within a molecule - constrained to a fixed net charge - while keeping the positions of the charges at atomic sites. This quite intuitive approach is usually called the Fluctuating Charge Model (FCM).[5–12] Unfortunately, its application is limited by the molecular geometry. For example, one cannot create out-of-plane charges in a planar molecule.

On the other hand, the permanent charges may be augmented by auxiliary charges or dipoles, the position or orientation of which is reactive to the environment. This idea has been realized in two concrete models: Induced Point-Dipoles (IPD)[13–20] and Drude Oscillators (DRU).[21–27] In the first case, mathematical dipoles located at atomic positions are calculated as a linear response to the local electric field. In other words, the strength of the induced dipoles is governed by a linear factor , i.e. the atomic polarisability. However, this implies that the traditional treatment of electrostatics based on point charges has to be extended to handle dipoles as well.[28,29] This initiated the idea of Drude oscillators: additional pairs of opposite charges are attributed to each atom. While one of these is united with the respective atom, the other one is tethered by a flexible spring. Its displacement is determined by the product of the atomic polarisability times the local field. Thus, the Drude pair creates an oscillating physical dipole.[21,27]

In this work, we aim for a critical comparison of the IPD and DRU models. As a test system we have chosen the molecular Ionic Liquid (IL) 1-ethyl-3-methylimidazolium ($EMIM^{\oplus}$) triflate ($CF_3SO_3^{\ominus}$) (cf. Fig. 1). In this class of soft matter every molecule carries a net charge. This leads to extraordinarily strong local electric fields, which in their turn create strong induced dipoles. This makes this investigation of dual interest. On the one hand, we are testing the IPD and DRU models up to their methodic limits. On the other hand, we focus on a system, where flexible electrostatics is essential.[25,30]

Implementing either the IPD or the DRU model is an extensive endeavor and implies a lot of additional algorithmic development.[27] The local electric field inducing the IPD or displacing the Drude charge does not only depend on the permanent charges, but also on the field *in situ* created by the other IPDs or Drude charges. Therefore, they have to be calculated in a self-consistent cycle. The final result of this process corresponds to the minimum of the polarisation energy. However, such a procedure is quite time-consuming. An economic alternative route is the Lagrange formalism,[21] which treats the IPDs or the positions of the Drude charges as additional degrees of freedom, for which appropriate equa-

[a)] Electronic mail: christian.schroeder@univie.ac.at

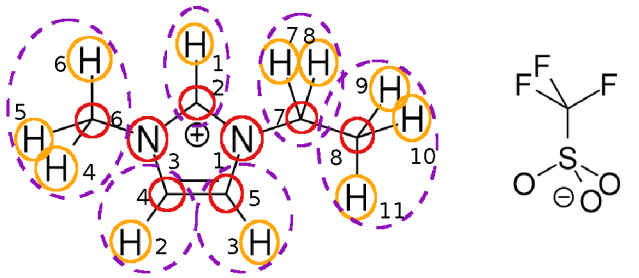

FIG. 1. Structures of the cation $EMIM^{\oplus}$ and the anion $CF_3SO_3^{\ominus}$ used in this work. This figure also shows the hydrogen polarisation models of the cation $EMIM^{\oplus}$. The circles illustrate which atoms are polarisable in the respective polarisation model: no hydrogen (only red), implicit hydrogen (purple), explicit hydrogen (red and orange).

tions of motion are solved. This requires fictitious masses or moments of inertia to be attributed to the Drude particles or IPDs, respectively. The two sets of equations of motion for the permanent and induced particles are formally treated identically. Their thermostats, however, operate at quite different temperatures. The purpose of the thermostat governing the inducible part of the system is to keep it near the minimum of the polarisation energy. Consequently, the temperature is usually kept below 1 K.[21] Despite this dual thermostating, inductive electrostatics needs to be damped at close distances to avoid an uncontrollable increase of polarisation. This is usually done within the framework of the Thole algorithm.[31] Because of algorithmic complexity, prominent simulation packages usually focus on implementing either the IPD or the Drude oscillator model. Therefore, we used AMBER[32] (for IPD) as well as CHARMM[33] (for DRU) in our comparative study. Therefore, one has to pay attention to the differences inevitably arising between these two simulation packages.

A first difference results from the question, whether hydrogen atoms can be made polarisable or not. This affects only the cation of the IL $EMIM^{\oplus}CF_3SO_3^{\ominus}$ chosen as our test system. While the IPD model in AMBER can explicitly handle polarisable hydrogen atoms, this cannot be done with the DRU model in CHARMM, as the hydrogen atoms and the Drude particles have comparable masses. This problem poses the second question, whether the hydrogen polarisability can be treated implicitly by adding it to the adjacent carbon atom. In this way, one can evade polarisable hydrogen atoms while still keeping the molecular polarisability the same. This creates four categories of polarisability distribution compared in this work. In the first case, all atoms are non-polarisable. Second, all non-hydrogen atoms are treated with their intrinsic polarisability. Third, all atoms are polarisable. And finally, the hydrogen polarisability is absorbed into the respective neighboring carbon atom. In the following, these four categories will be referred to as none, non-hydrogen, explicit hydrogen and implicit hydrogen.

1-ethyl-3-methyl-imidazolium				**Triflate**	
Atom	no H	implicit H	explicit H	Atom	α
N1	0.97157	0.97157	0.97157	C1	1.28860
C2	1.28860	1.70243	1.28860	F1	0.44475
N3	0.97157	0.97157	0.97157	F2	0.44475
C4	1.28860	1.70243	1.28860	F3	0.44475
C5	1.28860	1.70243	1.28860	S1	2.47445
H1	-	-	0.41383	O1	0.85197
H2	-	-	0.41383	O2	0.85197
H3	-	-	0.41383	O3	0.85197
C6	1.28860	2.53009	1.28860		
H4	-	-	0.41383		
H5	-	-	0.41383		
H6	-	-	0.41383		
C7	1.28860	2.11626	1.28860		
H7	-	-	0.41383		
H8	-	-	0.41383		
C8	1.28860	2.53009	1.28860		
H9	-	-	0.41383		
H10	-	-	0.41383		
H11	-	-	0.41383		
Sum	9.67474	14.22687	14.22687		7.65321

TABLE I. Atomic polarisabilities[34] for the cation in the various polarisation models and the anion. The numbering of the atoms of the cation is shown in Fig. 1. Values are given in units of $Å^3$.

II. METHODS

A. Simulation setup

This study is based on polarisable Molecular Dynamics (MD) simulations of the IL $EMIM^{\oplus}CF_3SO_3^{\ominus}$. The parameters for the bonded and non-bonded interactions of the force field were taken from Pádua *et al.*[35,36]. The respective atomic polarisabilities for the above-mentioned four models are based upon Ref. 34 and are collected in Tab. I. As this study is focused on a systematic study of different polarisability models, a possible recalibration of Lennard-Jones parameters was not done in order to keep parameter changes at a minimum.[25] With these values as a common input, we realized a suite of four polarisation models in AMBER 11[32] and three in CHARMM 38a2[33], where the explicit hydrogen model cannot be implemented. In addition to non-polarisable simulations, a series of polarisable simulations for each model was performed, thereby gradually changing the atomic polarisabilities in steps of ten percent up to their full value. Altogether, this comprised 52 simulations of varying length between 10 and 30 ns.

A non-polarisable system of 500 ion pairs in a cubic box was generated with PACKMOL.[37] After 20000 steps of energy minimization, a NpT equilibration run was performed at 300 K using the Berendsen barostat set to a reference pressure of 1 bar with a coupling constant of 1 ps, yielding an optimized box size of 54.6 Å. The final configuration served as the starting point for all subsequent NVT simulation runs. A uniform time step of

0.5 fs was used in all simulations. All bonds containing hydrogen atoms were constrained using the SHAKE algorithm[38]. The simulations were performed under periodic boundary conditions. Consequently, all electrostatic interactions were treated with the Particle Mesh Ewald method[39,40] using cubic splines of order 6 and a κ of 0.41 Å^{-1}. A grid with a spacing of approximately 1 Å was used in both cases. Instead of an SCF procedure to minimise the polariation energy, the Lagrange formalism was used with a dual thermostat keeping the system temperature near 300 K and the inducible part of the system below 1 K. The fictitious mass of the IPDs and the Drude particles were both set to 0.2 amu. A uniform Drude particle charge of $q^{\delta} = 2$ e was chosen. For the thermostat settings, the respective program default settings were used, i.e. Nosé-Hoover with τ=0.1 ps (300K) and τ=5 fs (1 K) in CHARMM and Berendsen with both τ set to 1 ps in AMBER.[41–44]

All analyses were carried out using a modified version of MDAnalysis[45]. Voronoi tessellations were calculated using the Voro++ library.[46]

B. Differences between CHARMM and AMBER

Before presenting the results, a brief summary of the differences between the IPD implementation in AMBER and the DRU implementation in CHARMM is given.

In the DRU model, the induced dipole moment $\vec{\mu}^{ind}_{i,\beta}$ assigned to atom β of molecule i is given by the product of the Drude charge q^{δ} times the displacement $\vec{d}_{i,\beta}$ of the two Drude particles. Speaking in terms of atomic polarisabilities α_{β}, $\vec{\mu}^{ind}_{i,\beta}$ is given by

$$\vec{\mu}^{ind}_{i,\beta} = \alpha_{\beta}\vec{E}_{i,\beta}. \quad (1)$$

The principle equivalence between the IPD and Drude models can be shown by the way the local electric field $\vec{E}_{i,\beta}$ acting on atom β of molecule i is computed. In the Drude model, we have

$$\vec{E}_{i,\beta} = \vec{E}^{0}_{i,\beta} + q^{\delta}\sum_{j}\sum_{\gamma}\left\{\frac{\vec{r}_{i,\beta}-\vec{r}_{j,\gamma}}{\mid \vec{r}_{i,\beta}-\vec{r}_{j,\gamma}\mid^{3}} - \frac{\vec{r}_{i,\beta}-(\vec{r}_{j,\gamma}+\vec{d}_{j,\gamma})}{\mid \vec{r}_{i,\beta}-(\vec{r}_{j,\gamma}+\vec{d}_{j,\gamma})\mid^{3}}\right\}, \quad (2)$$

where the summation runs over all Drude pairs γ of molecule j located at $\vec{r}_{j,\gamma}$ and $\vec{r}_{j,\gamma}+\vec{d}_{j,\gamma}$. The field exerted by the permanent charges is given by

$$\vec{E}^{0}_{i,\beta} = \sum_{j}\sum_{\gamma} q_{j,\gamma}\frac{\vec{r}_{i,\beta}-\vec{r}_{j,\gamma}}{\mid \vec{r}_{i,\beta}-\vec{r}_{j,\gamma}\mid^{3}}. \quad (3)$$

For small displacements $\vec{d}_{j,\gamma}$, one can use the truncated Taylor expansion

$$\frac{\vec{r}_{i,\beta}-(\vec{r}_{j,\gamma}+\vec{d}_{j,\gamma})}{\mid \vec{r}_{i,\beta}-(\vec{r}_{j,\gamma}+\vec{d}_{j,\gamma})\mid^{3}} = \frac{\vec{r}_{i,\beta}-\vec{r}_{j,\gamma}}{\mid \vec{r}_{i,\beta}-\vec{r}_{j,\gamma}\mid^{3}} + \overleftrightarrow{T}_{\beta\gamma}(\vec{r}_{i,\beta}-\vec{r}_{j,\gamma})\cdot\vec{d}_{j,\gamma}+\ldots \quad (4)$$

with the dipole-dipole tensor

$$\overleftrightarrow{T}_{\beta\gamma}(\vec{r}_{i,\beta}-\vec{r}_{j,\gamma}) = \vec{\nabla}_{j,\gamma}\vec{\nabla}_{j,\gamma}\frac{1}{\mid \vec{r}_{i,\beta}-\vec{r}_{j,\gamma}\mid}. \quad (5)$$

Inserting Eq. 4 into Eq. 2 one gets

$$\vec{E}_{i,\beta} = \vec{E}^{0}_{i,\beta} + \sum_{j}\sum_{\gamma}\overleftrightarrow{T}_{\beta\gamma}(\vec{r}_{i,\beta}-\vec{r}_{j,\gamma})\cdot\vec{\mu}^{ind}_{j,\gamma}, \quad (6)$$

with the induced dipole $\vec{\mu}^{ind}_{j,\gamma} = q^{\delta}\vec{d}_{j,\gamma}$. Eq. 6 describes the IPD model. As long as the Taylor expansion in Eq. 4 is valid, it is equivalent to the Drude model in Eq. 2. Although the pair of Drude charges represents a physical dipole, it corresponds to a mathematical one, i.e. the IPD model, for small displacements. According to Eq. 1, higher atomic polarisabilities induce higher dipole moments in the IPD model or larger displacements in the Drude model. This deteriorates the validity of Eq. 4 and inevitably leads to deviations between physical and mathematical dipoles.

Simulations of polarisable systems may be prone to instabilities, if the short-range interaction between induced dipoles is not dampened. The Thole algorithm[31] provides a framework to achieve this and is implemented in most simulation packages, but the respective functional form and the threshold for its range may differ. Tab. II of Ref. 47 lists the most frequently used forms of Thole functions $\phi(r)$. The default settings of AMBER and CHARMM, which are $\phi_1(r)$ or $\phi_3(r)$, respectively, were used for the simulations presented here. AMBER would offer the possibility to use the same functional form $\phi_3(r)$, but CHARMM and AMBER would still differ with respect to the threshold of the range of the Thole functions. Because of this, the default settings of CHARMM and AMBER were kept.

As the Lagrange formalism requires a dual thermostat, as discussed above, and CHARMM and AMBER differ considerably in this regard, this may also be a source of differences. The elaborate Nosé-Hoover thermostat was used in CHARMM, which reliably kept both temperature baths close to the desired mean values. The Berendsen thermostat used in AMBER was not so accurate in this regard. At the highest levels of atomic polarisability, there was some heat exchange between the two baths with some flow of kinetic energy towards the induced dipoles, raising the temperature to a few K. This had a slight influence on the dynamics of the respective systems. Other parameters than the default settings did not improve this either. Therefore, we kept the default setting for all systems to maintain consistency.

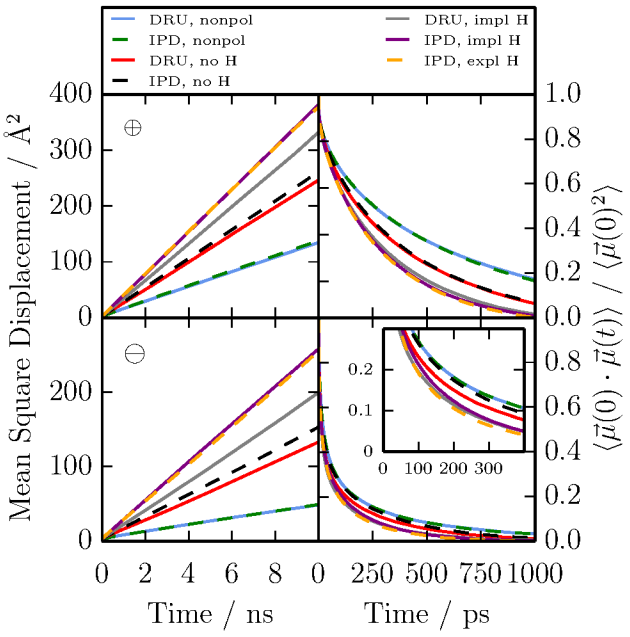

FIG. 2. This figure shows a comparison of the single-particle dynamics for different polarisation models in CHARMM (DRU) and AMBER (IPD). The left column shows the single-particle mean square displacement, the right columns shows the normalised permanent dipole autocorrelation function. The upper row shows cation dynamics, the lower row anion dynamics. The inset in the lower right graph is a magnification to highlight the pattern of polarisation models.

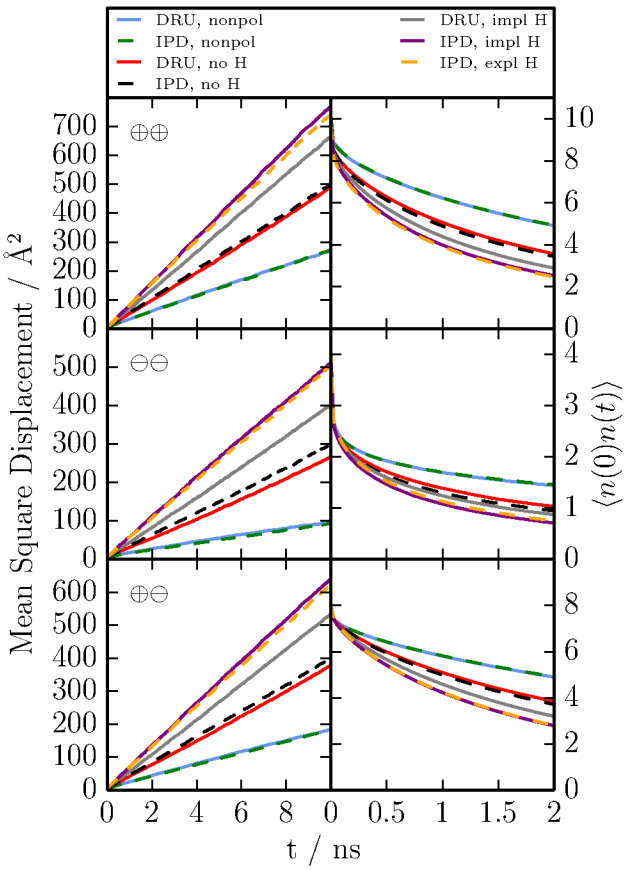

FIG. 3. A comparison of pair and cage dynamics for different polarisability models implemented with the DRU and IPD models. The left column shows the mean square pair displacement $\langle[\vec{R}_{ij}(t) - \vec{R}_{ij}(0)]^2\rangle$, the right column shows the cage relaxation function $\langle n(0)n(t)\rangle$ of the first solvation shell with the initial value being the average coordination number $\langle CN\rangle$. The upper row shows the functions for cations with respect to other cations, the middle row for anions with respect to other anions and the lower row for cations with respect to anions or vice versa.

III. RESULTS AND DISCUSSION

The following selection of results represents a mixture of traditionally given quantities in simulations of soft matter as well as other properties that were found to be quite indicative of the influence of polarisability. Thereby, the data are viewed from a threefold perspective: the systematic variation of polarisability in steps of ten percent, the difference between the IPD and DRU models and the question of the necessity of hydrogen polarisability.

A. Dynamics

As a first example, the mean square displacement (MSD) of the center-of-mass and the reorientation correlation function of the molecular dipole moment are given as typical representatives of single-particle translational and rotational motion. As done throughout this work, the numerical data were fitted to appropriate models of molecular motion to allow for better quantification of the influence of polarisability. In the case of single-particle translation, the model function

$$\langle[\vec{R}_i(t) - \vec{R}_i(0)]^2\rangle \cong 6D\sqrt{(t+\tau_0)^2 - \tau_0{}^2} \qquad (7)$$

previously used in Ref. 48 is applied. Throughout this work, the $\langle \dots \rangle$ bracket notation is a shorthand for the ensamble average. Here, $\vec{R}_i(t)$ are the molecular center-of-mass coordinates at time t, D is the diffusion coefficient and τ_0 accounts for the non-linear behaviour at short times. τ_0 is a measure of the time required for the displacement to become linear. To describe single-particle rotation, the permanent dipole moment $\vec{\mu}_i$ of each molecule i was used. Since the species have a net charge, the molecular dipole moment depends on the origin of the chosen reference system. In accordance with earlier works,[49] each dipole moment is referenced to the respective molecular center of mass. Average values of the permanent dipole moment of $EMIM^{\oplus}$ and $CF_3SO_3^{\ominus}$ are 0.69 D and 6.37 D, respectively. The corresponding normalised time correlation function was fitted to a

	CHARMM						AMBER								
	no H			impl H			no H			impl H			expl H		
scale	$D^{\oplus}$	$\tau^{\oplus}_{avg}$	$\eta_{\oplus}$	$D^{\oplus}$	$\tau^{\oplus}_{avg}$	$\eta_{\oplus}$	$D^{\oplus}$	$\tau^{\oplus}_{avg}$	$\eta_{\oplus}$	$D^{\oplus}$	$\tau^{\oplus}_{avg}$	$\eta_{\oplus}$	$D^{\oplus}$	$\tau^{\oplus}_{avg}$	$\eta_{\oplus}$
0.0	2.16	625	71.3				2.24	643	66.9						
0.1	2.26	600	68.2	2.40	609	61.6	2.62	568	56.1	2.55	577	57.8	2.57	569	57.7
0.2	2.49	585	59.9	2.52	547	60.7	2.43	566	63.0	2.56	558	58.7	2.76	522	54.1
0.3	2.76	516	54.4	2.77	510	54.4	2.63	575	55.5	2.80	527	52.7	3.13	464	47.6
0.4	2.93	534	49.0	3.00	503	48.7	2.82	544	51.5	3.03	502	48.1	3.58	431	40.4
0.5	2.97	510	49.1	3.51	448	40.8	3.01	499	48.5	3.22	466	45.4	4.00	412	34.9
0.6	3.21	493	44.5	3.46	443	41.8	3.18	492	45.2	3.56	434	40.5	4.26	380	33.1
0.7	3.44	472	40.9	3.88	410	36.6	3.49	478	39.9	4.19	393	33.3	4.82	353	28.5
0.8	3.39	434	43.5	4.15	369	34.9	4.39	379	31.7	5.76	304	23.5	5.97	283	23.1
0.9	3.63	418	40.1	4.23	345	35.2	4.34	394	31.6	5.62	299	24.6	6.03	288	22.6
1.0	4.08	412	33.9	5.49	314	24.9	4.24	423	31.6	6.36	297	20.5	6.29	284	21.3

TABLE II. The pseudo-viscosity $\eta_{\oplus}$ calculated from $D^{\oplus}$ and $\tau^{\oplus}_{avg}$ of the cation EMIM$^{\oplus}$ using Eq. 12. $D^{\oplus}$ is given in units of 10^{-11} m^2 s^{-1}, $\tau^{\oplus}_{avg}$ in units of ps and $\eta_{\oplus}$ in units of mPa s.

Kohlrausch-William-Watts (KWW) function of the form

$$\frac{\langle \vec{\mu}_i(t) \cdot \vec{\mu}_i(0) \rangle}{\langle \vec{\mu}_i(0)^2 \rangle} \cong e^{-(t/\tau)^{\beta}}. \tag{8}$$

This type of stretched exponential function characterises the diversity of dynamical processes by a single parameter β. Furthermore, an average τ can be obtained by the analytical expression

$$\tau_{avg} = \frac{\tau}{\beta} \Gamma\left(\frac{1}{\beta}\right), \tag{9}$$

where Γ is the gamma function. The respective fit parameters are collected in Tabs. S1 and S2 in the Supplementary Material. Graphs of the results from the non-polarisable simulations and those performed at full strength of the respective polarisability models are shown in Fig. 2. As a general rule, dynamics is accelerated with increasing polarisability and a clear pattern can be found. First, AMBER and CHARMM yield equivalent results for the non-polarisable force field, both, in translation and rotation. Second, comparing the DRU and IPD polarisation models for the case of non-polarisable hydrogen atoms in terms of their implementation in CHARMM and AMBER, one still finds almost equivalent results. Third, upon implicit inclusion of hydrogen polarisability, i.e. absorbing it into the respective neighboring carbon atom, the results of CHARMM and AMBER start to deviate. As can be seen from Tab. I, the implicit hydrogen model leads to very high polarisabilities of the carbon atoms, in some cases even exceeding that of sulfur. Considering Eqs. 1 - 6, it is shown that the DRU and IPD models must deviate beyond some threshold of polarisability. This seems to be the case here. Within AMBER, however, it does not matter whether hydrogen polarisability is modelled implicitly or explicitly, as both give equivalent results. Anyway, inclusion of hydrogen polarisability considerably raises the total sum of atomic polarisabilities, simply because of their large number (cf. Tab. I). As a consequence, dynamics is accelerated accordingly.

The pattern described above can be found as well in the cases of pair dynamics and cage dynamics (see Fig. 3). Pair dynamics[48] is characterised by the mean square displacement of the center-of-mass distance of two molecules i and j

$$\begin{aligned} \langle [\vec{R}_{ij}(t) - \vec{R}_{ij}(0)]^2 \rangle = \\ \langle [\vec{R}_i(t) - \vec{R}_i(0)]^2 \rangle + \langle [\vec{R}_j(t) - \vec{R}_j(0)]^2 \rangle \\ - 2\langle [\vec{R}_i(t) - \vec{R}_i(0)] \cdot [\vec{R}_j(t) - \vec{R}_j(0)] \rangle. \end{aligned} \tag{10}$$

Again, the functional form given in Eq. 7 was used for fitting. The resulting parameters are collected in Tabs. S3 and S4 in the Supplementary Material. The data show clearly that the pair diffusion coefficient D^{ij} is the sum of the respective self diffusion coefficients $D^{ij} = D^i + D^j$. In other words, the cross-term appearing in Eq. 10 is negligible.[48] It is important to note, that this additivity holds for all polarisation models across all scales (cf. Tabs. S3 and S4 in the Supplementary Material). Combined with earlier findings,[48] the disappearance of cross-terms in the pair dynamics of binary ionic liquids seems to be a general rule. This is of importance for model theories of pair dynamics based on this assumption, e.g. model theories of the Nuclear Overhauser Effect in NMR spectroscopy.[48,50]

By cage dynamics, the relaxation of the solvation shell of a reference molecule is meant. In this case, the solvation shell is defined as the first Voronoi shell,[46,51] comprising all molecules with Delaunay distance one. A binary observable $n(t)$ is defined, depending on whether a molecule is at time t a member of a given Voronoi cage or not. The respective time correlation function $\langle n(0)n(t) \rangle$ is shown in Fig. 3. The initial value of this residence function is the average coordination number $\langle CN \rangle$, i.e. the average number of particles located within the first solvation shell. After subtracting the steady-state asymptotic value a_0, the integral is the mean residence time τ_{cage}. The fit function[51]

$$\langle n(0)n(t) \rangle \cong a_1 \, e^{-t/\tau_1} + (\langle CN \rangle - a_1) \, e^{-(t/\tau_2)^{\beta}} + a_0 \tag{11}$$

was used. Except for the $\ominus\ominus$ residence function, a_1 could be set to zero. The respective fit parameters are listed in Tabs. S5 and S6 in the Supplementary Material.

As shown above, the polarisability pattern appears in various aspects of dynamics: single-particle translation and rotation, pair displacement and cage residence function. This raises the question whether these properties may be traced back to a common quantity. For this purpose we used the hydrodynamical relationship[52]

$$\eta_{\oplus} = \frac{k_B T}{3\pi\sqrt{6}} \frac{1}{\sqrt{(D^{\oplus})^3 \tau_{avg}^{\oplus}}} \tag{12}$$

to convert the diffusion coefficient $D^{\oplus}$ and the average reorientational time $\tau_{avg}^{\oplus}$ of the cation EMIM$^{\oplus}$ to a pseudo-viscosity $\eta_{\oplus}$, which is not to be understood as the collective viscosity of the system. Here, $\eta_{\oplus}$ serves as a scaling factor for dynamical parameters involving the cations such as $1/D^{\oplus}$, $\tau_{avg}^{\oplus}$, $1/D^{\oplus\oplus}$, $1/D^{\oplus\ominus}$, $\tau_{cage}^{\oplus\oplus}$ and $\tau_{cage}^{\oplus\ominus}$. As such, $\eta_{\oplus}$ behaves much like the actual collective viscosity η, which can be applied as a global scaling factor for dynamical properties in homogeneous systems.[52] Rescaling the aforementioned dynamical parameters with $\eta_{\oplus}$, one finds almost uniform values across all polarisability scales. In other words, the influence of polarisability on dynamical parameters can be mapped to the underlying variations of the $\eta_{\oplus}$, i.e. $1/D^{\oplus} = c * \eta_{\oplus}$ etc. The applicability of Eq. 12 rests upon the constancy of the product $D^{\oplus} \cdot \tau_{avg}^{\oplus}$ inferred from hydrodynamics, which is fairly valid for EMIM$^{\oplus}$, but not for $CF_3SO_3^{\ominus}$. Because of this, dynamical parameters involving only the anions scale less well, e.g. $\tau_{cage}^{\ominus\ominus}$, as will be discussed later. The resulting values for $\eta_{\oplus}$ are collected in Tab. II and graphically illustrated in Fig. 4. Thereby, not the scaling factor 0.0...1.0, but the total sum of the respective atomic polarisabilities of a single ion pair was used to compare polarisation models on a common scale. Inspired by the findings of Seddon *et al.*[53], that experimental viscosities follow an exponential law independent of the polarity of the added co-solvent, this law was adapted to the influence of polarisability on $\eta_{\oplus}$. The respective fit functions of the various polarisation models are also shown in Fig. 4. Indeed, all polarisation models, be they DRU or IPD, follow this experimentally inspired law and thus support the concept that polarisability acts as an inner solvent or co-solvent. Moreover, the DRU and IPD models lead to quite similar fit parameters, showing that they produce the same effects on dynamical observables.

As viscosity scaling stems from hydrodynamic diffusion tensors[52], its applicability is limited to time scales, where a system is diffusive in character. The model function given in Eq. 7 already indicates the typical non-diffusive behaviour exhibited by ionic liquids in the short-time regime. In order to gain a deeper insight, we have computed the van Hove self-correlation function[54,55] $G_s(r,t)$. This function shows the probability distribtion of the distance a given particle can travel within a certain time interval. The thick lines in Fig. 5 show this function for

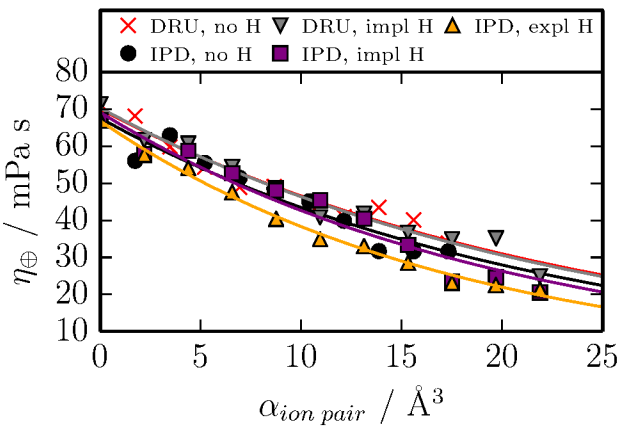

FIG. 4. $\eta_{\oplus}$ is shown as a function of the sum of the respective atomic polarisabilities of an ion pair for the various polarisation models with the corresponding experimentally inspired fit function of the form $\eta_{\oplus} \cong a\ e^{-x/b}$. The fit parameters for the different models are: DRU, no H (a=70.0, b=24.5); DRU, impl H (a=70.3, b=24.0); IPD, no H (a=67.6, b=22.7); IPD, impl H (a=69.1, b=20.7); IPD, expl H (a=66.8, b=18.0).

all polarisation models at time t = 1 ns. With increasing total polarisability of the model, the distribution of accessible distance widens and the maximum of the distribtion shifts to higher distances, thus reflecting the increasing fluidity of the system. For a purely diffusive behaviour, one would expect $G_s(r,t)$ to follow a Gaussian form[54]

$$G_s^0(r,t) = \left(\frac{3\pi}{2}\langle|\Delta\vec{r}(t)|^2\rangle\right)^{\frac{3}{2}} e^{-3r^2/(2\langle|\Delta\vec{r}(t)|^2\rangle)}. \tag{13}$$

The corresponding curves are shown as dashed lines in Fig. 5. As a measure of the deviation of the actual data from Gaussian behaviour, one usually computes the non-Gaussian parameter:[54,56]

$$a(t) = \frac{3}{5}\frac{\langle|\Delta\vec{r}(t)|^4\rangle}{\langle|\Delta\vec{r}(t)|^2\rangle^2} - 1. \tag{14}$$

The larger $a(t)$ becomes, the more pronounced is the non-Gaussian behaviour of the system. As can be seen from the insets in Fig. 5, $a(t)$ reaches a maximum at very short times and then decays monotonically. For more complex polarisability models, this maximum clearly shifts to shorter times and also the decay is enhanced. In other words, the system comes closer to Gaussian behaviour and is thus more diffusive in character. Again, it is important to note, that the implicit and the explicit hydrogen models behave almost identically.

While the dynamics of the cation EMIM$^{\oplus}$ could be mapped to $\eta_{\oplus}$, an analogous procedure for the anion did not work well. To further elucidate this, the non-Gaussian diffusive behaviour of the anions has to be studied. It can be quantified by two parameters, $\tau_0^{\ominus}$ of Eq. 7 and the time t_{max}, where $a(t)$ (cf. Eq. 14) reaches its

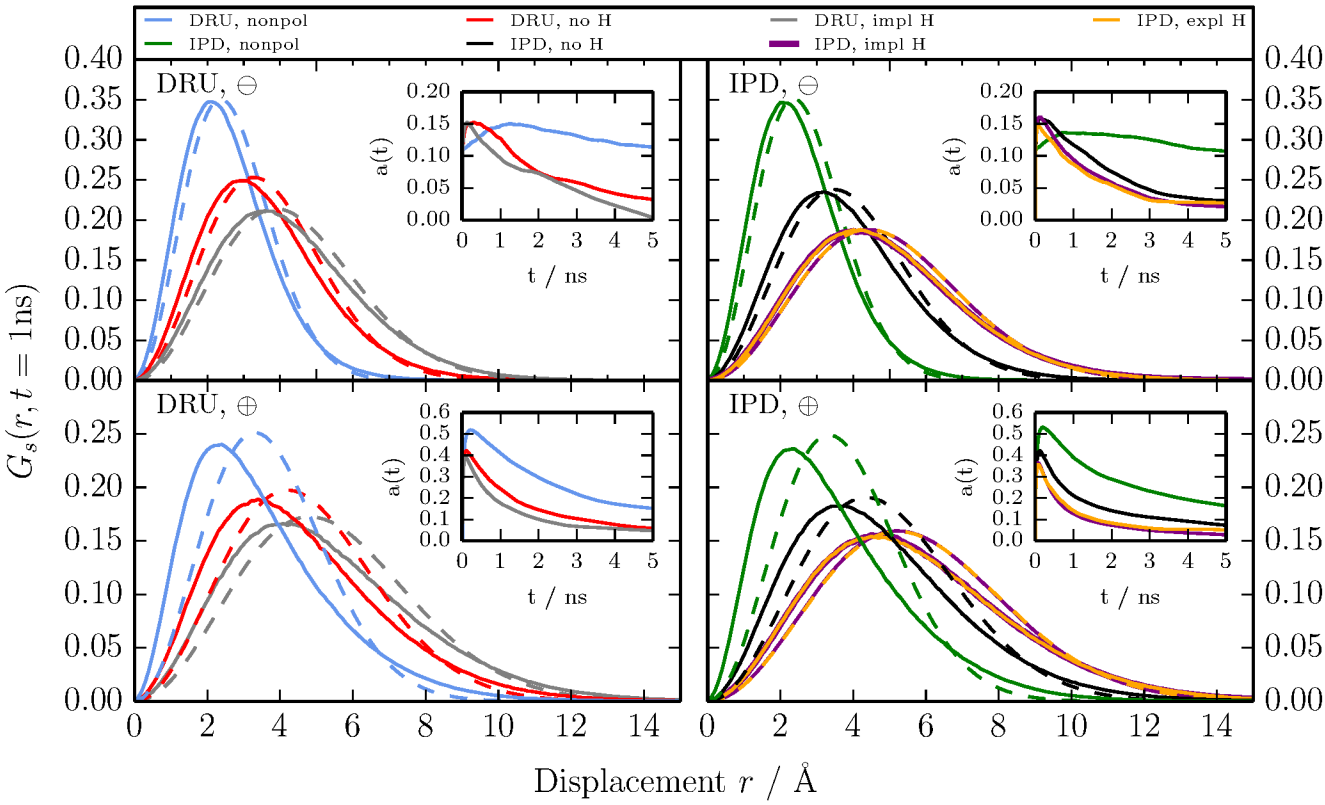

FIG. 5. The van Hove self-correlation function $G_s(r,t)$[54,55] is shown as the thick lines for the different polarisation models in CHARMM and AMBER for a time interval of 1 ns. The respective expected Gaussian forms $G_s^0(r,t)$ (cf. Eq. 13) are shown as dashed lines of the same color. The insets show the functional form of the corresponding non-Gaussian parameter $a(t)$ (cf. Eq. 14).

maximum. Both parameters are a measure for the time interval needed to enter the Gaussian diffusive regime. Indeed, they are pretty close in absolute value, bearing in mind that both are difficult to determine. This raises the question, how the Gaussian and non-Gaussian diffusive regimes are correlated. In fact, Fig. 6 shows strong correlation between $1/D^{\ominus}$ and $\tau_0^{\ominus}$. In other words, the slower translational motion is, the longer it takes to reach the Gaussian diffusive regime. The fact that even $\tau_0^{\ominus}$ or t_{max} is proportional to $1/D^{\ominus}$ across all polarisability scales highlights the central role of the diffusion coefficient for the dynamics of the anions. Indeed, also $\tau_{avg}^{\ominus\ominus}$ can be rescaled following $1/D^{\ominus}$ (see Fig. 6). Therefore, while viscosity scaling across polarisability scales is not possible for anion dynamics due to the different rates of change of $D^{\ominus}$ and $\tau_{avg}^{\ominus}$ (cf. Tabs. S1 and S2 in the Supplementary Material), scaling by $D^{\ominus}$ is a working substitute.

B. Structure

From cage dynamics we have learned that the initial value of the residence function $\langle n(0)n(t)\rangle$, representing the average coordination number $\langle CN\rangle$, is rather insensitive to polarisability. However, coordination numbers are integrals of solvation shell-resolved pair correlation functions $g^{000}(r)$ between molecular centers-of-mass R_{ij}. Consequently, a possible dependence of $g^{000}(r)$ on polarisability may compensate upon integration. Therefore, $g^{000}(r)$ for the combinations $\oplus\oplus$, $\ominus\ominus$ and $\oplus\ominus$ is studied at full radial resolution

$$g^{000}(r) = \frac{1}{\rho\, 4\pi r^2 dr} \sum_{j=1}^{N} \langle \delta(r - |R_{ij}|)\rangle. \qquad (15)$$

This function measures the deviation of the local particle density within a spherical shell of thickness dr from the uniform particle density ρ and thus is an indicator of molecular packing. The mutual orientation of molecules at a distance R_{ij} is characterised by

$$g^{110}(r) = \frac{1}{\rho\, 4\pi r^2 dr} \sum_{j=1}^{N} \left\langle \frac{\vec{\mu}_i \cdot \vec{\mu}_j}{|\vec{\mu}_i| \cdot |\vec{\mu}_j|} \delta(r - |R_{ij}|) \right\rangle, \qquad (16)$$

where $\vec{\mu}_i$ and $\vec{\mu}_j$ are the respective permanent molecular dipole moments. $g^{110}(r)$ is an extension of $g^{000}(r)$ in that it weights the local density by the cosine of the angle between the two dipole vectors.[49]

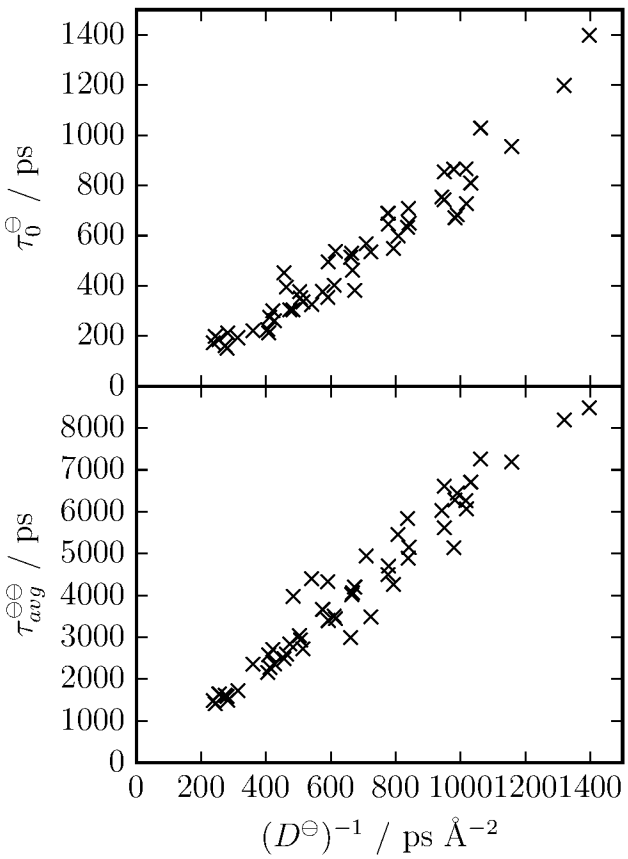

FIG. 6. Scatter plots showing the correlation of $1/D^{\ominus}$ to $\tau_0^{\ominus}$ (upper panel) and $\tau_{avg}^{\ominus\ominus}$ (lower panel) for all polarisation models in CHARMM and AMBER.

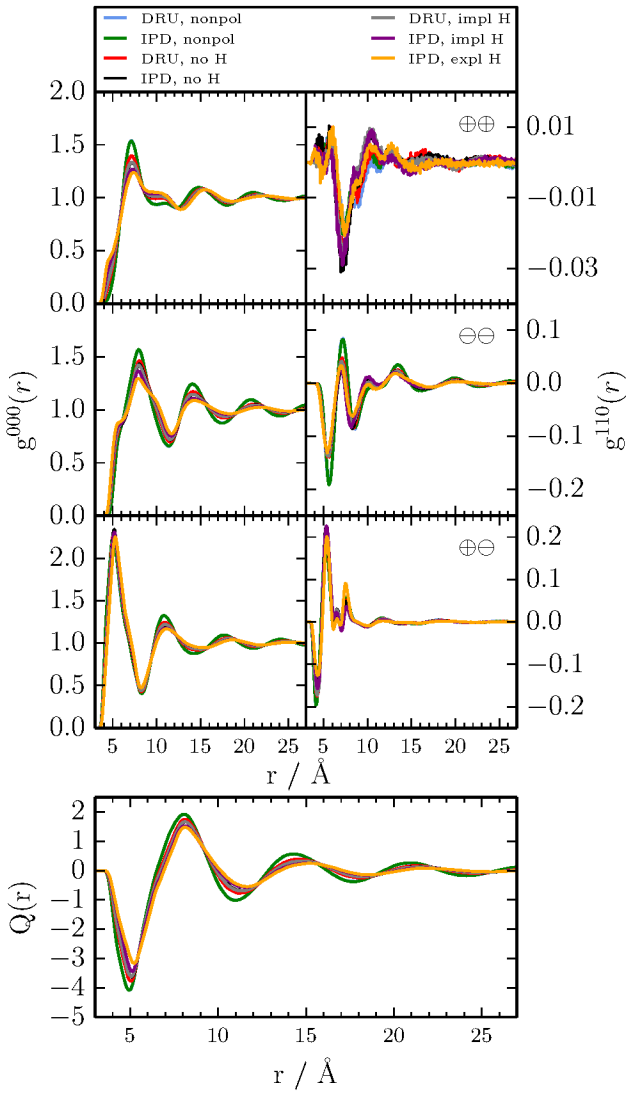

FIG. 7. The left column of the upper panel shows the functional form of the radial distribution function $g^{000}(r)$, the right column of the upper panel shows the orientational correlation function $g^{110}(r)$. Both are given for the center-of-mass distances of each, cations around cations, anions around anions or cations around anions or vice versa. The lower panel shows the charge ordering function $Q(r)$. All functions are shown for the non-polarisable case and at full strength of all polarisation models, each in CHARMM and AMBER.

The respective graphs of $g^{000}(r)$ and $g^{110}(r)$ are given in Fig. 7. For the purpose of discussion, three regions may be discerned: the immediate short range below 5 Å, the region around the highest peak from 5 to 10 Å and the long range order beyond 10 Å. With increasing polarisability, a shoulder emerges in the immediate short range for like species, $\oplus\oplus$ and $\ominus\ominus$, while at the same time, the highest peak is reduced in height. This corresponds to the concept of polarisability acting as an inner solvent by screening the repulsive electrostatic forces between like-charged molecules. For unlike charges $\oplus\ominus$, $g^{000}(r)$ below 10 Å is largely unaffected by polarisability changes. Without polarisable hydrogen atoms, the DRU and IPD models largely agree. Including hydrogen polarisability explicitly or implicitly further pronounces the effects described above with even stronger effects in the explicit case. However, for implicit hydrogen polarisability, CHARMM and AMBER deviate.

In the asymptotic region beyond 10 Å, the set of $g^{000}(r)$ functions exhibit an increasingly regular pattern of structural oscillations. The individual onset of this behaviour goes along with the vanishing of the orientational correlation function $g^{110}(r)$. For unlike charges, orientational structure disappears at shorter distances than for like charges, although it should be noted that $g^{110}_{\oplus\oplus}$ shows almost no correlation. Since a fortuitous 90 degree conformation - nullifying the cosine - has been ruled out by further analysis (data not shown), this effect comes from a lack of orientational steering between the cations caused by their comparatively small dipole moment. If the onset of the regular oscillation pattern in packing correlates with the vanishing of orientational correlation, then this behaviour can be interpreted as the transition from that of anisotropic molecular ions to

	CHARMM								AMBER											
	no H				impl H				no H				impl H				expl H			
scale	A	$1/\sigma$	λ	ϕ	A	$1/\sigma$	λ	ϕ	A	$1/\sigma$	λ	ϕ	A	$1/\sigma$	λ	ϕ	A	$1/\sigma$	λ	ϕ
0.0	30.0	0.087	6.43	25.1					29.8	0.086	6.42	25.1								
0.1	30.2	0.089	6.44	25.1	30.1	0.089	6.45	25.1	30.0	0.088	6.45	25.1	30.3	0.090	6.44	25.1	30.3	0.090	6.44	25.1
0.2	30.5	0.091	6.46	25.1	30.6	0.092	6.46	25.1	30.4	0.091	6.45	25.1	30.6	0.093	6.47	25.1	30.8	0.093	6.46	25.1
0.3	30.6	0.093	6.47	25.1	31.0	0.096	6.48	25.1	30.8	0.094	6.47	25.1	31.1	0.098	6.49	25.1	31.1	0.097	6.48	25.1
0.4	30.9	0.096	6.47	25.1	31.0	0.098	6.49	25.1	31.3	0.098	6.49	25.1	31.2	0.102	6.51	25.0	31.3	0.100	6.49	25.1
0.5	30.9	0.096	6.49	25.1	31.6	0.102	6.51	25.1	31.4	0.101	6.50	25.1	31.9	0.108	6.55	25.1	32.1	0.105	6.53	25.1
0.6	31.0	0.099	6.50	25.1	31.6	0.104	6.53	25.1	31.9	0.105	6.52	25.1	32.2	0.112	6.57	25.0	32.8	0.112	6.55	25.1
0.7	31.6	0.103	6.51	25.1	32.2	0.109	6.55	25.1	32.3	0.109	6.54	25.1	32.3	0.117	6.60	25.0	33.2	0.117	6.57	25.1
0.8	32.0	0.107	6.53	25.1	32.2	0.111	6.56	25.1	32.3	0.112	6.56	25.1	32.6	0.123	6.63	25.0	33.6	0.124	6.61	25.1
0.9	32.3	0.110	6.54	25.1	32.4	0.114	6.54	25.0	33.2	0.118	6.59	25.1	33.2	0.130	6.66	25.0	34.6	0.132	6.65	25.1
1.0	32.4	0.112	6.56	25.1	32.7	0.120	6.61	25.1	33.5	0.123	6.62	25.1	33.8	0.138	6.68	25.0	35.4	0.140	6.70	25.1

TABLE III. Parameters of the fit to the charge ordering function $Q(r)$ using the fit function $Q_{fit}(r)$ (cf. Eqs. 17 and 18) for all polarisation models in CHARMM and AMBER.

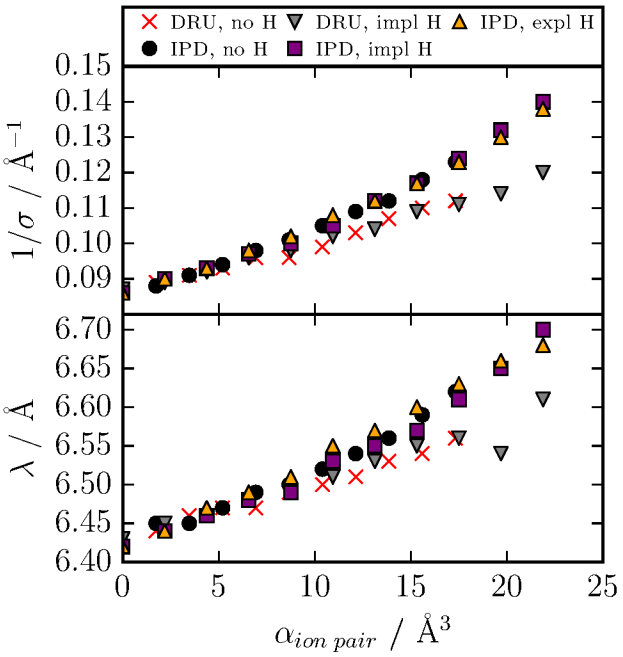

FIG. 8. The charge ordering function fit parameters $1/\sigma$ and λ (cf. Eq. 18) shown as a function of the total sum of the respective atomic polarisabilities for all polarisability models in CHARMM and AMBER.

pseudo-spherical ions. In the latter case, the oscillations of like and unlike ions are synchronised with a coincidence of respective maxima and minima. The charge ordering function

$$Q(r) = g^{000}_{\oplus\oplus}(r) + g^{000}_{\ominus\ominus} - 2g^{000}_{\oplus\ominus} \tag{17}$$

by design rationalizes this oscillation pattern and is a measure of the surplus or deficit of like charged ions at distance r. $Q(r)$ can be fitted to the function[57]

$$Q_{fit}(r) = \frac{A}{r} e^{-r/\sigma} sin\left(\frac{2\pi r}{\lambda} + \phi\right). \tag{18}$$

As this function only describes the oscillating pattern just discussed, the fit can only be used beyond some threshold, in our case 5 Å. The respective fit parameters are collected in Tab. III. The functions $Q(r)$ shown for selected systems in the lower panel of Fig. 7 illustrate the effect of polarisability. Quite intriguingly, the two hydrogen models, implcit and explicit, give a highly similar form of $Q(r)$. This shows, that for longer distances, the individual location of the hydrogen polarisabilities is less relevant than for shorter distances, but their inclusion is important nonetheless. As a general feature, increase of polarisability dampens the oscillations of the function. This can be quantified by the fit parameter $1/\sigma$, which increases monotonically. When again plotted as a function of the total sum of the polarisabilities of an ion pair, only two separate curves are observed (cf. the upper panel of Fig. 8). All hydrogen polarisability models - none, implicit or explicit - lie on the same curve, the only difference being between CHARMM and AMBER, i.e. between the DRU and IPD models. The overall trend for both models is quite the same, but it is less pronounced in CHARMM. Still, damping alone is not a sufficient description of the observed changes: when integrating over successive radial shells $\int_0^\infty Q(r) 4\pi r^2 dr$, the final cumulative value has to be independent of the polarisation model. This balance is conserved by the increase of the wavelength of the oscillations, described by the fit parameter λ (cf. the lower panel of Fig. 8), which shows the same pattern for the DRU and IPD models as $1/\sigma$. A higher λ shifts the peaks of $Q(r)$ slightly outwards, where they are weighted with a higher r^2. In this way, the higher dampening is compensated. Thus, with increasing polarisability and the ensuing screening of electrostatic interaction, the long range charge ordering is less pronounced. In this sense, inductive effects make an ionic liquid behave more like a neutral molecular liquid.

IV. CONCLUSION

In this paper, the influence of polarisability on the structure and dynamics of liquid systems is studied, using the ionic liquid EMIM$^{\oplus}$CF$_3$SO$_3^{\ominus}$as a test case. Three aspects have been highlighted: a systematic variation of the strength of polarisability, a comparison of the Drude oscillator model (DRU) and the induced point-dipole model

(IPD) as implemented in CHARMM and AMBER, respectively as well as the special influence of hydrogen polarisability.

Concerning the variation of the polarisability, the total sum of polarisabilities of an ion pair turned out to be the common scale for the various polarisability models. The general influence of polarisability is to make the liquid more fluid and less structured. The effect on dynamics can be rationalized by introducing a common scaling factor $\eta_{\oplus}$, derived from hydrodynamical relationships involving the cationic diffusion coefficient $D^{\oplus}$ and reorientational time $\tau_{avg}^{\oplus}$. As the variation of many dynamical observables with increasing polarisability can be mapped to corresponding changes in $\eta_{\oplus}$, it may serve as a central quantity representing dynamics. The systematic loss of structure was quantified using the charge ordering function $Q(r)$ as a measure of alternating charge layers. Its behaviour upon raising the polarisability can be characterised by a pair of parameters, the damping factor $1/\sigma$ and the wavelength λ. From these parameters one can read, that the alternating charge layers increase in width. This partial penetration reduces maxima and minima of $Q(r)$. Thus, an increase in polarisability creates screening of electrostatic interaction and leads to a loss of long-range order. However, inclusion of polarisability does not change the short-range structural features of the liquid in a qualitative manner. In fact, these features are only less pronounced due to the aforementioned electrostatic screening. Both the damping of the structure as well as the increase in dynamics may be attributed to this screening. As the molecular packing becomes looser and the particles gain more freedom to move, dynamics is accelerated significantly, but the accessible configurations remain quite the same.

When comparing the different hydrogen polarisability models - non-polarisable, explicitly polarisable or implicitly polarisable hydrogen atoms - the importance of their inclusion becomes obvious. The way of inclusion - explicitly or implicitly - is not so important. This opens up the possibility to include hydrogen polarisability in the DRU model, where explicitly polarisable hydrogen atoms are methodically unfeasible. As the inclusion of hydrogens raises the total sum of polarisabilities, the effects on structure and dynamics described above are further increased according to this common scale.

With respect to the method of implementing polarisability - the DRU model in CHARMM or the IPD model in AMBER - it could be shown, that both models are equivalent at least in a qualitative sense. Trends in all observables are highly similar, although the results begin to deviate at the highest polarisability levels. This is most obvious, when comparing the implicit hydrogen model, where the highest atomic polarisabilities are achieved, between CHARMM and AMBER. Generally, the IPD model in AMBER seems to have a slightly higher impact on the observables described here.

In addition to the principle equivalence of the Drude oscillator and the induced point-dipole models, the inclusion of polarisability in general may be seen as adding an inner solvent or co-solvent, in that via screening electrostatic interactions, dynamics is accelerated and structure is loosened.

ACKNOWLEDGMENT

We would like to thank the Vienna Scientific Cluster (http://www.zid.tuwien.ac.at/vsc) for the generous allocation of computer time. This work was funded by the Austrian Science Fund FWF in the context of Project No. P23494,by the Cost Action CM 1206: "Exchange on ionic liquids" and the SafeBatt project of the BMBF (Project No. 03X4631N).

[1] M. P. Allen and D. J. Tildesley, *Computer simulations of liquids* (Oxford Press, New York, 1989).
[2] L. Verlet, Phys. Rev. **159**, 98 (1967).
[3] U. Singh and P. Kollman, J. Comput. Chem. **5**, 129 (1984).
[4] H. Yu and W. F. van Gunsteren, Comput. Phys. Commun. **172**, 69 (2005).
[5] S. W. Rick, S. J. Stuart, and B. J. Berne, J. Chem. Phys. **101**, 6141 (1994).
[6] S. Patel and C. L. Brooks III, J. Comput. Chem. **25**, 1 (2004).
[7] A. K. Rappe and W. A. Goddard III, J. Phys. Chem. **95**, 3358 (1991).
[8] M. C. C. Ribeiro, Phys. Rev. B **63**, 094205 (2001).
[9] A. de Oliveira Cavalcante, M. Ribeiro, and M. Skaf, J. Chem. Phys. **140**, 144108 (2014).
[10] H. A. Stern, F. Rittner, B. J. Berne, and R. A. Friesner, The Journal of Chemical Physics **115**, 2237 (2001).
[11] S. W. Rick, The Journal of Chemical Physics **114**, 2276 (2001).
[12] S. Zhu, S. Singh, and G. W. Robinson, The Journal of Chemical Physics **95**, 2791 (1991).
[13] T. Yan, C. J. Burnham, M. G. Del Pópolo, and G. A. Voth, J. Phys. Chem. B **108**, 11877 (2004).
[14] W. Jiang, T. Yan, Y. Wang, and G. A. Voth, J. Phys. Chem. B **112**, 3121 (2008).
[15] T. Yan, Y. Wang, and C. Knox, J. Phys. Chem. B **114**, 6886 (2010).
[16] T. Yan, Y. Wang, and C. Knox, J. Phys. Chem. B **114**, 6905 (2010).
[17] T.-M. Chang and L. X. Dang, J. Phys. Chem. A **113**, 2127 (2009).
[18] O. Borodin, J. Phys. Chem. B **113**, 11463 (2009).
[19] O. Borodin, W. Gorecki, G. Smith, and M. Armand, J. Phys. Chem. B **114**, 6786 (2010).
[20] J. B. Hooper, O. N. Starovoytov, O. Borodin, D. Bedrov, and G. D. Smith, J. Chem. Phys. **136**, 194506 (2012).
[21] G. Lamoureux and B. Roux, J. Chem. Phys. **119**, 3025 (2003).
[22] H. Yu, T. Hansson, and W. F. van Gunsteren, J. Chem. Phys. **118**, 221 (2003).
[23] E. Harder, V. M. Anisimov, I. V. Vorobyov, P. E. M. Lopes, S. Y. Noskov, A. D. MacKerell Jr., and B. Roux, J. Chem. Theory Comput. **2**, 1587 (2006).
[24] D. P. Geerke and W. F. van Gunsteren, J. Chem. Theory Comput. **3**, 2128 (2007).
[25] C. Schröder and O. Steinhauser, J. Chem. Phys. **133**, 154511 (2010).
[26] C. Schröder, Phys. Chem. Chem. Phys. **14**, 3089 (2012).
[27] P. E. M. Lopes, B. Roux, and A. D. MacKerell Jr., Theor. Chem. Acc. **124**, 11 (2009).
[28] H. Kornfeld, Zeitschrift für Physik **22**, 27 (1924), ISSN 0044-3328.
[29] D. Adams and G. Dubey, Journal of Computational Physics **72**, 156 (1987), ISSN 0021-9991.

[30]D. Bedrov, O. Borodin, Z. Li, and G. D. Smith, J. Phys. Chem. B **114**, 4984 (2010).
[31]B. T. Thole, Chem. Phys. **59**, 341 (1981).
[32]D. A. Case, T. A. Darden, T. E. Cheatham, III, C. Simmerling, J. Wang, R. E. Duke, R. Luo, R. C. Walker, W. Zhang, K. Merz, et al., *Amber 11*, San Francisco (2010).
[33]B. R. Brooks, C. L. Brooks III, A. D. MacKerell Jr., L. Nilsson, R. J. Petrella, B. Roux, Y. Won, G. Archontis, C. Bartels, S. Boresch, et al., J. Comput. Chem. **30**, 1545 (2009).
[34]P. T. van Duijnen and M. Swart, J. Phys. Chem. A **102**, 2399 (1998).
[35]J. N. Canongia Lopes, J. Deschamps, and A. A. H. Pádua, J. Phys. Chem. B **108**, 2038 (2004).
[36]J. N. Canongia Lopes and A. A. H. Pádua, J. Phys. Chem. B **108**, 16893 (2004).
[37]L. Martínez, R. Andrade, G. Birgin, and J. M. Martínez, J. Comput. Chem. **30**, 2157 (2009).
[38]J.-P. Ryckaert, G. Ciccotti, and H. J. C. Berendsen, J. Comput. Phys. **23**, 327 (1977).
[39]T. Darden, D. York, and L. Pedersen, J. Chem. Phys. **98**, 10089 (1993).
[40]U. Essmann, L. Perera, M. L. Berkowitz, T. Darden, H. Lee, and L. G. Pedersen, J. Chem. Phys. **103**, 8577 (1995).
[41]H. Berendsen, J. Postma, W. van Gunsteren, A. DiNola, and J. Haak, J. Chem. Phys. **81**, 3684 (1984).
[42]S. Nosé, Mol. Phys. **52**, 255 (1984).
[43]S. Nosé, J. Chem. Phys. **81**, 511 (1984).
[44]W. G. Hoover, Phys. Rev. **A31**, 1695 (1985).
[45]N. Michaud-Agrawal, E. J. Denning, T. B. Woolf, and O. Beckstein, J. Comput. Chem. **32**, 2319 (2011).
[46]C. Rycroft, G. Grest, J. Landry, and M. Bazant, Phys. Rev. E **74**, 021306 (2006).
[47]T. Taylor, M. Schmollngruber, C. Schröder, and O. Steinhauser, J. Chem. Phys. **138**, 204119 (2013).
[48]S. Gabl, C. Schröder, D. Braun, H. Weingärtner, and O. Steinhauser, J. Chem. Phys. **140**, 184503 (2014).
[49]C. Schröder, T. Rudas, G. Neumayr, W. Gansterer, and O. Steinhauser, J. Chem. Phys. **127**, 044505 (2007).
[50]S. Gabl, O. Steinhauser, and H. Weingärtner, Angew. Chem. Int. Ed. **52**, 9242 (2013).
[51]G. Neumayr, C. Schröder, and O. Steinhauser, J. Chem. Phys. **131**, 174509 (2009).
[52]D. Braun, S. Boresch, and O. Steinhauser, J. Chem. Phys. **140**, 064107 (2014).
[53]K. R. Seddon, A. Stark, and M.-J. Torres, Pure Appl. Chem. **72**, 2275 (2000).
[54]M. G. Del Pópolo and G. A. Voth, J. Phys. Chem. B **108**, 1744 (2004).
[55]L. van Hove, Phys. Rev. **95**, 249 (1954).
[56]A. Rahman, Phys. Rev. **136**, A405 (1964).
[57]M. Haberler, C. Schröder, and O. Steinhauser, J. Comput. Theory Chem. **8**, 3911 (2012).